A&A, 708, L2 (2026)
https://doi.org/10.1051/0004-6361/202558660

Astronomy & Astrophysics

LETTER TO THE EDITOR

A faint $M_{UV} = -14.5$ Lyman-continuum leaker candidate in the epoch of reionization: Unprecedented Lyα properties at $z = 5.725$

M. Messa[1,⋆], E. Vanzella[1], T. Morishita[2,3], M. Stiavelli[4], T. Treu[5], P. Bergamini[1], Z. Liu[6,7], A. Zanella[1], A. Bolamperti[8], A. Verhamme[9,10], T. Garel[10,9], C. Grillo[11,12], and P. Rosati[13,1]

[1] INAF – OAS, Osservatorio di Astrofisica e Scienza dello Spazio di Bologna, Via Gobetti 93/3, I-40129 Bologna, Italy
[2] IPAC, California Institute of Technology, Pasadena, CA 91125, USA
[3] Astronomical Institute, Tohoku University, 6-3 Aramaki, Aoba-ku, Sendai 980-8578, Japan
[4] Space Telescope Science Institute (STScI), 3700 San Martin Drive, Baltimore, MD 21218, USA
[5] Department of Physics and Astronomy, University of California, Los Angeles, 430 Portola Plaza, Los Angeles, CA 90095, USA
[6] MIT Kavli Institute for Astrophysics and Space Research, 70 Vassar Street, Cambridge, MA 02139, USA
[7] Astronomical Institute, Graduate School of Science, Tohoku University, Sendai, Miyagi 980-8578, Japan
[8] Max-Planck-Institut für Astrophysik, Karl-Schwarzschild-Str. 1, D-85748 Garching, Germany
[9] Univ Lyon, Univ Lyon1, ENS de Lyon, CNRS, Centre de Recherche Astrophysique de Lyon UMR5574, Saint-Genis-Laval, France
[10] Observatoire de Genève, Université de Genève, Chemin Pegasi 51, 1290 Versoix, Switzerland
[11] Dipartimento di Fisica, Università degli Studi di Milano, Via Celoria 16, I-20133 Milano, Italy
[12] INAF – IASF Milano, Via A. Corti 12, I-20133 Milano, Italy
[13] Dipartimento di Fisica e Scienze della Terra, Università degli Studi di Ferrara, Via Saragat 1, I-44122 Ferrara, Italy

Received 18 December 2025 / Accepted 27 February 2026

ABSTRACT

We report the unprecedented Lyα properties of AMORE6, an extremely metal-poor ($12 + \log(O/H) < 6$), low-mass ($M_\star = 4.4 \times 10^5\, M_\odot$), and ultracompact (effective radius ~30 pc) dwarf galaxy at $z = 5.7253$, which is gravitationally lensed by the cluster A2744. A prominent, narrow, and nearly symmetric Lyα emission line is detected at the systemic redshift (the latter traced by Hβ, from JWST/NIRCam slitless spectroscopy), with a rest-frame equivalent width of 150 ± 10 Å, a full width at half maximum of 58 ± 1 km s^{-1}, and a slight asymmetry, resulting in a flux excess of ~10% in the red wing of the line. The negligible velocity offset from systemic ($dv = 4 \pm 67$ km s^{-1}, 3σ uncertainty), together with the sharpness and symmetry of the profile, indicates minimum radiative transfer effects, which implies a neutral hydrogen column density consistent with an optically thin medium that in turn is compatible with a nonzero ionizing photon escape fraction. If indirect spectral diagnostics calibrated at $z < 4.5$ remain the only viable tools for identifying LyC leakers during reionization, then based on its strongest indicator (Lyα), AMORE6 stands out as one of the most compelling LyC-leaking candidates yet discovered in the epoch of reionization.

Key words. radiative transfer – galaxies: high-redshift

1. Introduction

The epoch of reionization (EoR) marks the last main phase transition of the Universe, when the first stars and galaxies revealed their presence by ionizing the surrounding neutral hydrogen (H I; e.g., Loeb & Furlanetto 2013). While the reionization timeline is increasingly well constrained ($z \simeq 6$–9; e.g., Fan et al. 2006; Mason et al. 2019, 2026; Planck Collaboration VI 2020), the nature of the dominant ionizing sources remains elusive. Faint, low-mass galaxies have been proposed as the primary contributors to the ionizing photon budget (e.g., Finkelstein et al. 2019; Simmonds et al. 2024), although the role of massive galaxies is not yet fully understood, as they may also produce substantial Lyman continuum (LyC) emission (e.g., Naidu et al. 2020; Marques-Chaves et al. 2024). Direct measurements of ionizing UV radiation ($\lambda < 912$ Å) are prevented at $z \gtrsim 4.5$ by the high opacity of the intergalactic medium (IGM Worseck et al. 2014; Inoue et al. 2014). Thus, current efforts focus on low-redshift LyC emitters (e.g., Flury et al. 2022a; Jaskot et al. 2024a) as analogs of $z > 6$ galaxies to calibrate indirect diagnostics of LyC leakage applicable in the EoR. Recent work highlighted the multiparameter nature of LyC leakage, requiring correlations with diverse physical properties to be established through multivariate approaches. For instance, Jaskot et al. (2024a), analyzed 35 local ($z \sim 0.3$) LyC emitters (Flury et al. 2022a,b) and identified several key diagnostics: the EW of Lyman absorption features, the UV β slope (see also Chisholm et al. 2022), Lyα peak separation and shift, the Lyα escape fraction (see also Dijkstra et al. 2016), dust excess $E(B-V)_{\rm neb}$, the star formation rate surface density, and the O32 index ([OIII]4959,5007/[OII]3727). These diagnostics have also been applied to a handful of confirmed LyC emitters at intermediate redshift ($1 < z < 4$; Jaskot et al. 2024b), and they now provide a framework for probing reionization-era sources, particularly with JWST access to rest-frame optical lines at $z = 6$–9 (e.g., Mascia et al. 2024). In parallel, radiative transfer models predict a tight connection between LyC escape and Lyα spectral properties (e.g., Behrens et al. 2014; Verhamme et al. 2015; Monter et al. 2026). Observations and radiative transfer models confirm that galaxies with multipeaked Lyα profiles and a narrow peak close to systemic are likely optically thin to LyC (e.g.,

⋆ Corresponding author: matteo.messa@inaf.it

Schaerer et al. 2011; Verhamme et al. 2017, 2018; Izotov et al. 2018, 2021; Vanzella et al. 2020; Naidu et al. 2022). The Lyα peak separation is controlled by the residual H I column density of the carved channels, and the line asymmetry correlates with the porosity and multiphase structure of the HII region (e.g., Kakiichi & Gronke 2021). However, the increasing IGM neutrality during the EoR (partially) suppresses and reshapes Lyα, limiting its diagnostic power (e.g., Pentericci et al. 2014; Garel et al. 2021; Mason et al. 2026). Mitigating cases arise for sources located in ionized bubbles around luminous $z \simeq 6$ quasars (e.g., Protušová et al. 2025) or along unusually transparent sightlines (Matthee et al. 2018), where double-peaked Lyα emission with a narrow peak separation has been observed up to $z \simeq 6.5$, pointing to nonzero LyC escape.

In this Letter, we revisit the extremely metal-poor source AMORE6, which was recently identified by Morishita et al. (2025) with $12 + \log(\mathrm{O/H}) < 6$, in the context of escaping ionizing radiation. AMORE6 is a remarkably faint ($M_{1700} \simeq -14.5$), compact ($R_{\rm eff} \sim 30$ pc) galaxy at $z = 5.725$ that is strongly magnified by the galaxy cluster A2744. Beyond its extraordinary low metallicity and luminosity, its unprecedented Lyα spectral properties provide compelling evidence for substantial ionizing photon escape at $z \simeq 6$, opening a new window on the nature of reionization-era galaxies. Throughout the Letter, we assume a flat cosmology with $\Omega_{\rm M} = 0.3$, $\Omega_\Lambda = 0.7$, and $H_0 = 70\,\mathrm{km\,s^{-1}\,Mpc^{-1}}$. All magnitudes are given in the AB system (Oke & Gunn 1983): $m_{\rm AB} = 23.9 - 2.5\log(f_\nu/\mu\mathrm{Jy})$.

2. Analysis

The analysis of the rest-optical spectrum[1], in particular, the Hβ emission, was presented by Morishita et al. 2025 (hereafter M25). The Hβ redshift from M25 is adopted here as the systemic redshift of AMORE6 (see Table 1); in a conservative approach, we considered its 3σ uncertainty. From the same analysis, the UV magnitude of the AMORE6-B counter-image and its UV β slope were used to estimate the expected continuum at the Lyα wavelength. The flux from image A is contaminated by the light from three foreground sources; for this reason, its magnitude was not reported by M25. In addition, image B has the strongest magnification ($\mu \simeq 77$, compared to $\mu \simeq 39$ for AMORE6-A; Bergamini et al. 2023), and thus, we considered AMORE6-B as the reference for this spectral analysis; we verified that the main results of this work remain unchanged when A is considered instead (see Table 1).

The analysis of the rest-UV spectrum was based on observations from the Multi Unit Spectroscopic Explorer (MUSE) and X-shooter instruments, on the Very Large Telescope (VLT). The MUSE data we used were described by Mahler et al. (2018) and Bergamini et al. (2023). X-shooter observations (PI T. Morishita, DDT, prog.id. 115.29G6.001) were carried out between August and September 2025 with a median seeing of $1.0^{+0.1}_{-0.2}$ arcsec for a total integration time on source of 11 h. The full dataset will be presented in a forthcoming work (Morishita et al. in prep.). Briefly, we used science ESO level 2 products, specifically focusing on the visual arm (VIS), where the Lyα lies. The Lyα emission is clearly detected in each OB with a signal-to-noise ratio S/N > 15. All OBs were visually inspected and aligned in four cases along the spatial direction by 1 pixel (measuring the Lyα peak), averaged, and the one-dimensional spectrum was extracted by centering on the source AMORE6-B from a window enclosing 10 spatial pixels (1.6″; Fig. 1). The spectrum was converted from air into vacuum reference wavelength and was then corrected to the barycentric radial velocity[2] (through `astropy`). The resulting Lyα emission sampled at a spectral resolution R ≃ 8900 is shown in Fig. 2. The line location is fully consistent with the location inferred from MUSE (see Table 1). The MUSE spectrum was also used to calibrate the X-shooter Lyα flux, in order to correct for the slit loss.

We fit the line with `specutils/astropy` using Gaussian profiles. The fit quantities are reported in Table 1.

Table 1. Lyα-related properties of AMORE6.

	B	A	B (MUSE)
$z_{\rm sys}^{(a)}$	5.7253	5.7253	5.7253
$\delta(z_{\rm sys})^{(a)}$	0.0015	0.0030	0.0015
$z_{\rm Ly\alpha}$	5.7254	5.7256	5.7256
$\delta(z_{\rm Ly\alpha})^{(b)}$	0.0001	0.0001	0.0001
dv [km s^{-1}]	4 ± 67	13 ± 147	13 ± 147
FWHM$_{\rm Ly\alpha}$ [Å]$^{(c)}$	1.83 ± 0.03	1.81 ± 0.04	3.06 ± 0.05
FWHM$_{\rm Ly\alpha}$ $\left[\frac{\rm km}{\rm s}\right]^{(d)}$	58.2 ± 1.4	57.1 ± 1.7	63.6 ± 3.2
$A_{\rm RB}{}^{(e)}$	$0.12^{+0.04}_{-0.05}$	$0.19^{+0.05}_{-0.08}$	$0.31^{+0.01}_{-0.01}$
$A_{\rm PERC}{}^{(e)}$	$0.11^{+0.06}_{-0.06}$	$0.24^{+0.10}_{-0.10}$	$0.06^{+0.01}_{-0.01}$
$f_{\rm Ly\alpha}$ [10^{-17}cgs]	2.32 ± 0.05	1.72 ± 0.06	2.32 ± 0.05
mag$_{\rm Ly\alpha,continuum}{}^{(f)}$	$27.14^{+0.07}_{-0.08}$	–	$27.14^{+0.07}_{-0.08}$
EW$_{\rm Ly\alpha}$ [Å]	150^{+10}_{-12}	–	150^{+10}_{-12}

Notes. The properties in Cols. 1 and 2 are taken from X-shooter data for images B and A, respectively; MUSE measurements for image B are also reported in Col. 3. (a) From M25; the uncertainty here is 3σ. NIRCam-WFSS at observed Hβ has R ∼ 1500, implying $\sigma_z \sim 0.004$, or $\sigma_{\rm v} \sim 200$ km s^{-1}. (b) 5σ uncertainty (see text). (c) Observed FWHM. (d) Instrument- corrected FWHM. (e) RB and PERC asymmetry as defined in the text. (f) $M_{\rm UV}$ from M25 extrapolated to the observed Lyα continuum using $\beta = -2.77$.

3. Results

Figure 2 shows the VLT/X-shooter Lyα line extracted from AMORE6-B; the line is detected at an S/N ≃ 40, centered at $\lambda = 8175.81 \pm 0.08$ Å (vacuum), corresponding to $z = 5.7254 \pm 0.0001$ (for a rest-frame Lyα wavelength of 1215.67 Å). The rest-frame equivalent width is 150 ± 10 Å. Two unprecedented properties emerge at this high redshift: (1) the velocity offset with respect the systemic redshift is $dv = 4 \pm 67$ km s^{-1}, which is fully consistent with emission located at the resonance frequency ($dv = 0$); (2) even at the high spectral resolution of X-shooter ($d\lambda \simeq 0.92$ Å, corresponding to ≃ 34 kms^{-1}), the line profile is nearly symmetric and narrow, with a measured FWHM of 1.83 ± 0.03 Å, or 58 ± 1 km s^{-1}, after correcting for instrumental broadening. The line is slightly asymmetric, which we quantified with the red/blue asymmetry parameter ($A_{\rm RB}$), that is, the flux difference redward and blueward of the observed line peak, normalized by the line flux; the value $A_{\rm RB} = 0.12^{+0.04}_{-0.05}$ indicates a flux excess of ∼10% on the red side of the line. Similar results emerge from the nonparametric percentile asymmetry parameter, defined as $A_{\rm PERC} = \frac{(\lambda_{90}-\lambda_{50})-(\lambda_{50}-\lambda_{10})}{(\lambda_{90}-\lambda_{10})}$, which shows $A_{\rm PERC} = 0.11 \pm 0.06$, which is still close to symmetry with a faint excess toward the red side. We point out that overall consistent results were obtained when the Lyα from the AMORE6-A image was considered (Table 1 for details). Although the spectral resolution is lower by 2.5 times, the analysis of the MUSE spectrum also recovers similar properties (Table 1).

[1] From the NIRCam WFSS Cycle 2 program "All the Little Things", GO 3516; PIs: Matthee & Naidu, (see Naidu et al. 2024).

[2] To make it consistent with the NIRCam-WFSS spectrum of M25.

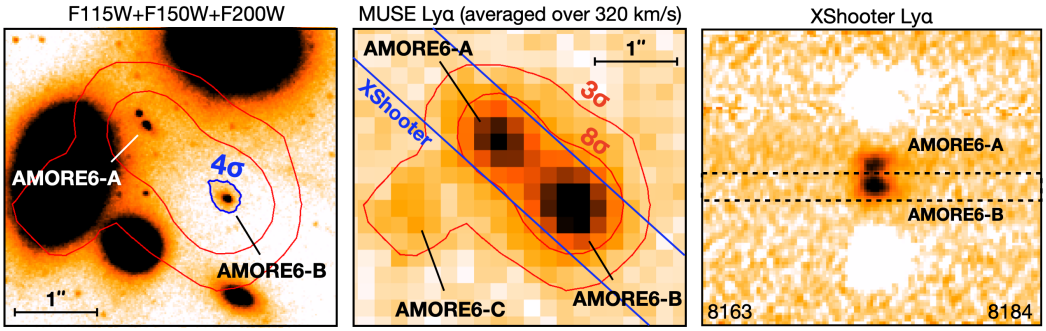

Fig. 1. Left: NIRCam stacking of the SW bands. The red contours highlight the extent of the Lyα emission, and the blue contour encloses the rest-UV emission of AMORE6-B. Middle: Lyα flux from VLT/MUSE; a faint emission from a low-magnification third counter-image (AMORE6-C) is also visible. Right: Zoomed two-dimensional X-shooter spectrum centered on the Lyα wavelength from 8163 Å to 8184 Å. The dotted lines show the region we used to extract spectra.

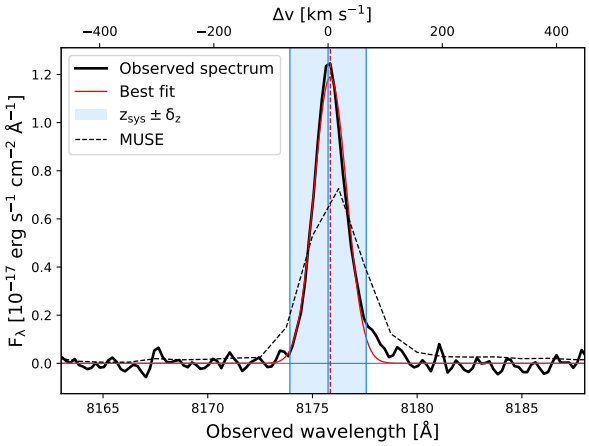

Fig. 2. Observed profile of the Lyα emission for AMORE6-B (black line), best-fit profile (solid red), best-fit central wavelength (dashed red), systemic redshift (and relative uncertainty) from Morishita et al. (2025, solid blue lines and shaded region). The (lower-resolution) MUSE spectrum is shown as the dashed black line.

These properties have never been observed so clearly at this redshift. Recently, Saxena et al. (2024) and Prieto-Lyon et al. (2025) identified few galaxies showing an emerging Lyα line at the systemic redshift (i.e., very small dv), within a large sample of Lyman-alpha emitters (LAEs) at $5 < z < 8$ (Appendix A). However, in most cases, the line profile is larger than what is measured in AMORE6 (FWHM $\gtrsim 200$ km s^{-1}) and the asymmetry is very pronounced, indicating the effect of gas reprocessing of the line. In the remaining cases, the S/N is too low for us to infer the line profiles. We point out that $z \gtrsim 4$ LAEs studied in the literature (including other galaxies magnified by gravitational lensing) are brighter by about 4–6 magnitudes than AMORE6, $M_{UV} \lesssim -18$ (see Appendix A). The comparison with confirmed LyC leakers at lower redshifts ($z \leq 4$) showing Lyα at the systemic velocity (e.g., Sunburst, Rivera-Thorsen et al. 2019 and Vanzella et al. 2022; Ion3, Vanzella et al. 2018 and Meštrić et al. 2025; Ion2, Vanzella et al. 2020), together with radiative transfer models (see below) indicates that AMORE6 might be the most promising LyC-leaking candidate known to date at $z \simeq 6$.

In dense HI environments, Lyα photons scatter until they shift out of resonance, producing broad profiles with little flux at systemic and widely separated peaks. In contrast, in AMORE6, all of the Lyα flux emerges close to resonance, suggesting extremely low column densities and likely ionized channels that perforate the ISM. In particular, given the steep ultraviolet slope ($\beta = -2.77$, $F_\lambda \propto \lambda^\beta$) and the extremely low metallicity ($12 + \log(O/H) < 6$; M25), the observed Lyα emission is expected to be negligibly affected by dust attenuation and only weakly affected by neutral gas damping. A similar conclusion can be inferred from radiative transfer (RT) models (e.g., Behrens et al. 2014; Almada Monter & Gronke 2024), which show that densities as low as $N_{HI} \gtrsim 10^{16}$ cm^{-2} are reflected in asymmetric and/or multipeaked Lyα profiles, displaced from the systemic redshift (in the expanding-shell scenario, with low to moderate expansion velocities, $v_{exp} \lesssim 100$ kms^{-1}; Verhamme et al. 2015, 2018; see our Appendix B). The optical depth of Lyα photons is indeed higher by $\sim 10^4$ times than that of LyC photons (e.g., Verhamme et al. 2015), and the detection of copious Lyα emission that peaks at the line center would therefore indicate column densities that are sufficiently low to imply a large escape fraction of ionizing photons ($f_{esc,LyC} \simeq 0.5$–1.0).

The low column density we derived might imply an ionized channel along the line of sight. Alternatively, the observed line profile might be the sign of a clumpy ISM with a low covering fraction. A perforated dense neutral ISM may still give rise to a double-peak profile that surrounds the central profle (e.g., Rivera-Thorsen et al. 2017; Almada Monter & Gronke 2024; Monter et al. 2026), as observed in some confirmed leakers, (e.g., Rivera-Thorsen et al. 2019; Vanzella et al. 2018, 2020). The absence of multiple Lyα peaks in the observed spectrum suggests that the ISM around AMORE6 has a low covering fraction overall. From simulations that coupled Lyα transfer with detailed radiation hydrodynamics in individual HII regions, Kakiichi & Gronke (2021) studied the interplay between Lyα and LyC escape and suggested that the shape of the main Lyα peak can distinguish between anisotropic LyC leakage through holes in a turbulent HII region (indicated by asymmetry within the red peak in a double-peaked profile) and isotropic LyC leakage from a fully density-bounded HII region (symmetric profile). AMORE6 would then represent the first likely example of an isotropic LyC emitter at $z \simeq 6$.

In this likely scenario, the narrow Lyα line resolved with X-shooter and its nearly symmetric profile suggest that the blue wing is only weakly affected by absorption of the intergalactic medium, which at $z = 5.7$ might otherwise attenuate more than 50% of the total line flux (e.g., Laursen et al. 2011). As reported by M25, AMORE6 lies between two known overdensities that are each separated by ~5 proper Mpc from the source. These structures might have generated an ionized region around AMORE6 that mitigates the expected IGM damping.

As a alternative to the main interpretation, RT models predict a relatively symmetric emission at systemic redshift at higher densities ($N_{HI} > 10^{17}$ cm^{-2}) in case of fast-expanding gas shells ($v_{exp} \gg 100$ km s^{-1}; Schaerer et al. 2011; see our Appendix B). Fast outflows like this are observed in massive and/or highly star-forming galaxies ($M \gtrsim 10^9$ M$_\odot$, SFR $\gtrsim 1$ M$_\odot$yr^{-1}; Chisholm et al. 2015). However, we recall that AMORE6 is intrinsically a small and low-mass system, that is, it is closer to a massive star cluster or compact HII region, for which velocities < 100 km s^{-1} are expected (e.g., Tenorio-Tagle et al. 2015; Turner et al. 2015). In addition, studies of local LyC emitters found that LAE systems with the narrowest Lyα profile (as in the case of AMORE6) show the lowest velocities (e.g., Jaskot et al. 2017).

Finally, a further possibility to explain the observed Lyα emission at $dv \approx 0$ km s^{-1} in case of high densities is a shift in the actual systemic redshift of AMORE6 by $\sim 100-200$ km s^{-1}; such a substantial difference would still be consistent with the redshift determined by M25 within 3σ, given the uncertainty associated with the Hβ line center (see Table 1). In this case, the observed Lyα would be a gas-processed red peak, where the absence of a blue peak might be attributed to the suppression by absorption from the IGM (e.g. Inoue et al. 2014; Garel et al. 2021). We stress, however, that even in this case, for gas densities $>10^{17}$ cm^{-2}, the observed line would broaden and likely become asymmetric (as shown in Appendix B); the narrow and almost symmetric profile of the Lyα line that is robustly characterized at high spectral resolution strongly disfavor this scenario.

4. Final remarks

AMORE6 is an exceptional source for several reasons: (1) its currently inferred metallicity is the lowest known among high-redshift galaxies, making it a prime candidate pristine star-forming region (M25); (2) it is strongly lensed by a factor of ~77 (Bergamini et al. 2023) and can therefore be spatially resolved down to ~30 pc in the image plane; and (3) it represents the most compelling case of a Lyman-continuum leaker candidate identified during the epoch of reionization (along with the z ~ 10 candidate from Marques-Chaves et al. 2026). Its Lyα emission properties are consistent with a HI column optically thin to LyC, which is indicative of a high global escape fraction.

Under these conditions, in which little (or no) radiative transfer reprocesses the Lyα line, its profile is expected to be consistent with the Balmer lines emitted from the same system. Unfortunately, as discussed in M25, the current low spectral resolution of Hβ from NIRCam-WFSS prevents a detailed comparison between the two. Deep NIRSpec observations with a high spectral resolution are needed to characterize the shape of the Balmer lines (and possibly measure the gas expansion velocity), to refine the systemic redshift, and to search for additional emission lines.

Acknowledgements. We thank the anonymous referee for the useful comments and suggestions which helped improving the draft. MM and EV acknowledge financial support through grants INAF GO Grant 2022 "The revolution is around the corner: JWST will probe globular cluster precursors and Population III stellar clusters at cosmic dawn" and INAF GO Grant 2024 "Mapping Star Cluster Feedback in a Galaxy 450 Myr after the Big Bang", and by the European Union – NextGenerationEU within PRIN 2022 project n.20229YBSAN - Globular clusters in cosmological simulations and lensed fields: from their birth to the present epoch. TM received support from NASA through the STScI grant JWST-GO-3990. MS acknowledges partial support through NASA grant 80NSSC21K1294. This research has used NASA's Astrophysics Data System, QFitsView, and SAOImageDS9, developed by Smithsonian Astrophysical Observatory. Additionally, this work made use of the following open-source packages for Python, and we are thankful to the developers of these: Matplotlib (Hunter 2007), Numpy (van der Walt et al. 2011), Astropy (Astropy Collboration 2022) (`http://www.astropy.org`).

References

Almada Monter, S., & Gronke, M. 2024, MNRAS, 534, L7
Astropy Collboration (Price-Whelan, A. M., et al.) 2022, ApJ, 935, 167
Behrens, C., Dijkstra, M., & Niemeyer, J. C. 2014, A&A, 563, A77
Bergamini, P., Acebron, A., Grillo, C., et al. 2023, ApJ, 952, 84
Chisholm, J., Tremonti, C. A., Leitherer, C., et al. 2015, ApJ, 811, 149
Chisholm, J., Saldana-Lopez, A., Flury, S., et al. 2022, MNRAS, 517, 5104
Claeyssens, A., Richard, J., Blaizot, J., et al. 2019, MNRAS, 489, 5022
Dijkstra, M., Gronke, M., & Venkatesan, A. 2016, ApJ, 828, 71
Fan, X., Carilli, C. L., & Keating, B. 2006, ARA&A, 44, 415
Finkelstein, S. L., D'Aloisio, A., Paardekooper, J.-P., et al. 2019, ApJ, 879, 36
Flury, S. R., Jaskot, A. E., Ferguson, H. C., et al. 2022a, ApJS, 260, 1
Flury, S. R., Jaskot, A. E., Ferguson, H. C., et al. 2022b, ApJ, 930, 126
Garel, T., Blaizot, J., Rosdahl, J., et al. 2021, MNRAS, 504, 1902
Garel, T., Michel-Dansac, L., Verhamme, A., et al. 2024, A&A, 691, A213
Hunter, J. D. 2007, Comput. Sci. Eng., 9, 90
Inoue, A. K., Shimizu, I., Iwata, I., & Tanaka, M. 2014, MNRAS, 442, 1805
Izotov, Y. I., Thuan, T. X., Guseva, N. G., & Liss, S. E. 2018, MNRAS, 473, 1956
Izotov, Y. I., Worseck, G., Schaerer, D., et al. 2021, MNRAS, 503, 1734
Jaskot, A. E., Oey, M. S., Scarlata, C., & Dowd, T. 2017, ApJ, 851, L9
Jaskot, A. E., Silveyra, A. C., Plantinga, A., et al. 2024a, ApJ, 972, 92
Jaskot, A. E., Silveyra, A. C., Plantinga, A., et al. 2024b, ApJ, 973, 111
Kakiichi, K., & Gronke, M. 2021, ApJ, 908, 30
Laursen, P., Sommer-Larsen, J., & Razoumov, A. O. 2011, ApJ, 728, 52
Loeb, A., & Furlanetto, S. R. 2013, The First Galaxies in the Universe
Mahler, G., Richard, J., Clément, B., et al. 2018, MNRAS, 473, 663
Mainali, R., Kollmeier, J. A., Stark, D. P., et al. 2017, ApJ, 836, L14
Marques-Chaves, R., Schaerer, D., Vanzella, E., et al. 2024, A&A, 691, A87
Marques-Chaves, R., Álvarez-Márquez, J., Colina, L., et al. 2026, A&A, submitted [arXiv:2602.02322]
Mascia, S., Pentericci, L., Calabrò, A., et al. 2024, A&A, 685, A3
Mason, C. A., Fontana, A., Treu, T., et al. 2019, MNRAS, 485, 3947
Mason, C. A., Chen, Z., Stark, D. P., et al. 2026, A&A, 705, A114
Matthee, J., Sobral, D., Gronke, M., et al. 2018, A&A, 619, A136
Messa, M., Dessauges-Zavadsky, M., Adamo, A., Richard, J., & Claeyssens, A. 2024, MNRAS, 529, 2162
Messa, M., Vanzella, E., Loiacono, F., et al. 2025, A&A, 694, A59
Meštrić, U., Vanzella, E., Beckett, A., et al. 2025, A&A, 698, A203
Monter, S. A., Gronke, M., & Chang, S. J. 2026, MNRAS, 547, stag330
Morishita, T., Liu, Z., Stiavelli, M., et al. 2025, ArXiv e-prints [arXiv:2507.10521]
Naidu, R. P., Tacchella, S., Mason, C. A., et al. 2020, ApJ, 892, 109
Naidu, R. P., Matthee, J., Oesch, P. A., et al. 2022, MNRAS, 510, 4582
Naidu, R. P., Matthee, J., Kramarenko, I., et al. 2024, Open J. Astrophys., submitted [arXiv:2410.01874]
Oke, J. B., & Gunn, J. E. 1983, ApJ, 266, 713
Pentericci, L., Vanzella, E., Fontana, A., et al. 2014, ApJ, 793, 113
Planck Collaboration VI. 2020, A&A, 641, A6
Prieto-Lyon, G., Mason, C. A., Strait, V., et al. 2025, A&A, submitted [arXiv:2509.18302]
Protušová, K., Bosman, S. E. I., Wang, F., et al. 2025, A&A, 700, A218
Rivera-Thorsen, T. E., Dahle, H., Gronke, M., et al. 2017, A&A, 608, L4
Rivera-Thorsen, T. E., Dahle, H., Chisholm, J., et al. 2019, Science, 366, 738
Saxena, A., Bunker, A. J., Jones, G. C., et al. 2024, A&A, 684, A84
Schaerer, D., Hayes, M., Verhamme, A., & Teyssier, R. 2011, A&A, 531, A12
Simmonds, C., Tacchella, S., Hainline, K., et al. 2024, MNRAS, 527, 6139
Swinbank, A. M., Webb, T. M., Richard, J., et al. 2009, MNRAS, 400, 1121
Tang, M., Stark, D. P., Ellis, R. S., et al. 2024, MNRAS, 531, 2701
Tenorio-Tagle, G., Muñoz-Tuñón, C., Silich, S., & Cassisi, S. 2015, ApJ, 814, L8
Turner, J. L., Beck, S. C., Benford, D. J., et al. 2015, Nature, 519, 331
van der Walt, S., Colbert, S. C., & Varoquaux, G. 2011, Comput. Sci. Eng., 13, 22
Vanzella, E., Nonino, M., Cupani, G., et al. 2018, MNRAS, 476, L15
Vanzella, E., Calura, F., Meneghetti, M., et al. 2019, MNRAS, 483, 3618
Vanzella, E., Caminha, G. B., Calura, F., et al. 2020, MNRAS, 491, 1093
Vanzella, E., Castellano, M., Bergamini, P., et al. 2022, A&A, 659, A2
Verhamme, A., Orlitová, I., Schaerer, D., & Hayes, M. 2015, A&A, 578, A7
Verhamme, A., Orlitová, I., Schaerer, D., et al. 2017, A&A, 597, A13
Verhamme, A., Garel, T., Ventou, E., et al. 2018, MNRAS, 478, L60
Witstok, J., Smit, R., Maiolino, R., et al. 2021, MNRAS, 508, 1686
Worseck, G., Prochaska, J. X., O'Meara, J. M., et al. 2014, MNRAS, 445, 1745

Appendix A: Literature samples of LAEs at z>4.

Recent studies by Tang et al. (2024), Saxena et al. (2024) and Prieto-Lyon et al. (2025) put together a large sample of LAEs, including Lyα line profiles, at similar redshifts to AMORE6. More specifically, Prieto-Lyon et al. (2025) first provided a statistical sample of Lyα FWHM at z $\sim$ 5–6. The main Lyα-related properties of these samples are shown in Fig. A.1. In addition various lensed LAEs in the same redshift range have been studied in the literature (though none intrinsically as faint as AMORE6); we collect their main properties and relative references in Table A.1. Overall, while few galaxies have a Lyα emission very close to the systemic redshift ($dv \sim 0$ km/s), AMORE6 is the only case with a narrow Lyα profile (FWHM < 100 km/s) robustly detected (right panel of Fig. A.1).

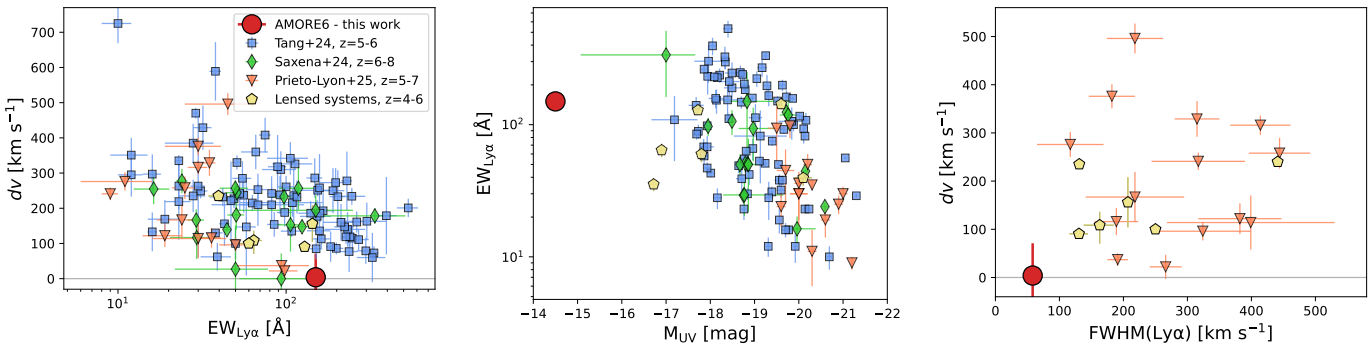

Fig. A.1. Comparison of the Lyα properties of AMORE6 with literature samples of galaxies at z > 4. *Left:* shift of the Lyα peak relative to systemic (dv) versus rest-frame Lyα EW; literature samples from Tang et al. (2024), Saxena et al. (2024), Prieto-Lyon et al. (2025); references for the lensed-galaxies sample in Table A.1. *Center:* EW(Lyα) versus M_{UV}; AMORE6 is 4 – 5 mag fainter than the comparison average. *Right:* dv versus $FWHM_{Ly\alpha}$ for cases with both measurements.

Table A.1. Lyα properties of lensed LAEs at z > 4 from the literature.

ID	z_{sys}	M_{UV}	$EW_{Ly\alpha}$	dv	FWHM
MACS0940	4.0338[a]	−19.8[b]	–	240 ± 7[a]	441 ± 8[a]†
RCS0224[c]	4.8737	−19.6	143.3 ± 12.9	156 ± 52	207 ± 6†
MS1358[d]	4.9296	−19.0 ± 0.1	–	200 ± 100	–
CA8[e]	6.064	−16.9 ± 0.1	64.2 ± 7.4	109^{+28}_{-38}	163^{+22}_{-25}
RXCJ2248[f]	6.1045	−20.1 ± 0.2	39.6 ± 5.1	235	131
CA4[e]	6.1446	−17.7 ± 0.1	128.8 ± 9.4	91^{+3}_{-4}	131^{+14}_{-15}
D1T1	6.1449[g]	−17.8 ± 0.1[g]	60 ± 8[h]	100[g]	250[g]†
CA5[e]	6.149	−16.7 ± 0.1	35.4 ± 4.0	–	176^{+110}_{-20}

Notes. Uncertainties are not reported when they are not available in the original publication. † not corrected for instrumental broadening.[a] Claeyssens et al. (2019); [b] Messa et al. (2024); [c] all data from Witstok et al. (2021); [d] all data from Swinbank et al. (2009); [e] all data from Bolamperti et al. in prep; [f] all data from Mainali et al. (2017); [g] Messa et al. (2025); [h] Vanzella et al. (2019).

Appendix B: Comparison to radiative transfer models

We fit AMORE6 with the grid of idealized Lyα radiative-transfer models from Garel et al. (2024) accounting for the instrumental broadening and identified two families of acceptable solutions, both implying very low effective opacity: (i) very fast outflows, or (ii) extremely low H I columns. Figure B.1 shows the best–fit models for each family, alongside variants in which all parameters are fixed to the best–fit values except N_{HI} (to illustrate its dominant impact on the Lyα profile).

In the high-velocity family, the preferred solution adopts $N_{HI} = 10^{20}$ cm^{-2} to reproduce the modest red wing; however faint residuals of this wing (almost consistent with the observational noise level) extend up to redder wavelengths than observed. Models with lower N_{HI} are essentially indistinguishable and recover the intrinsic line shape because the effective opacity is negligible, whereas higher N_{HI} suppress near–systemic photons and fail to match the data. However, such an extreme outflow ($V_{max} \approx 750$ km s^{-1}) is probably unlikely for an HII region/star cluster (e.g., Turner et al. 2015; Tenorio-Tagle et al. 2015). Restricting the search to $V_{max} \leq 100$ km s^{-1}, good fits are obtained only with very low columns, with a best fit at $N_{HI} \approx 10^{14}$ cm^{-2}; larger densities inevitably shifts the Lyα peak redward of systemic and degrades the fit. Under the hypothesis of low velocity of the expanding shell, this strongly indicates that the line–of–sight N_{HI} in AMORE6 is extremely low, consistent with a high LyC escape fraction.

A caveat is the IGM opacity at this redshift, which is not included in our forward models and could attenuate the blue side of the line. The observed profile's near symmetry suggests this effect is modest, but it does not alter the conclusion that AMORE6 exhibits very low effective neutral columns.

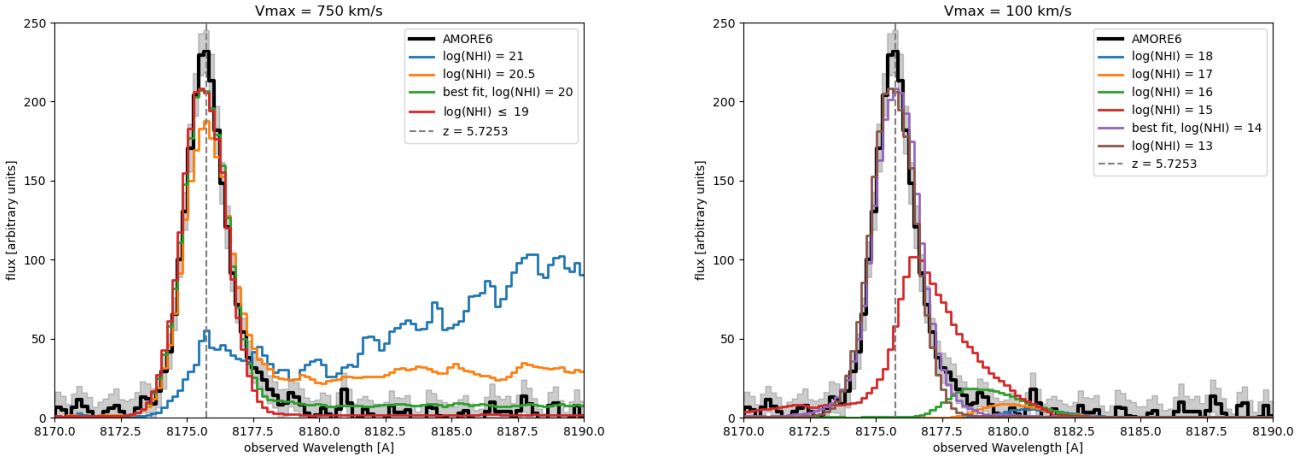

Fig. B.1. Emergent Lyα line profiles from a grid of idealized radiative-transfer models (see text). Left: high-velocity shell (V_{max} = 750 km s^{-1}); varying N_{HI} shows that log(N_{HI}) $\lesssim$ 20 reproduces the observed profile but requires an extreme outflow. Right: low-velocity case (V_{max} = 100 km s^{-1}); matching the data demands very low columns, log(N_{HI}) $\lesssim$ 14. Both panels assume the systemic redshift z = 5.7253.